First publ. in: Nucleic Acids Research 38 (2010), 3, e14
doi:10.1093/nar/gkp932

Published online 11 November 2009

Specific local induction of DNA strand breaks by infrared multi-photon absorption

D. Träutlein[1], M. Deibler[2], A. Leitenstorfer[1] and E. Ferrando-May[2,*]

[1]Department of Physics and [2]Department of Biology and Center for Applied Photonics, University of Konstanz, D-78457 Konstanz, Germany

Received June 26, 2009; Revised October 6, 2009; Accepted October 11, 2009

ABSTRACT

Highly confined DNA damage by femtosecond laser irradiation currently arises as a powerful tool to understand DNA repair in live cells as a function of space and time. However, the specificity with respect to damage type is limited. Here, we present an irradiation procedure based on a widely tunable Er/Yb : fiber femtosecond laser source that favors the formation of DNA strand breaks over that of UV photoproducts by more than one order of magnitude. We explain this selectivity with the different power dependence of the reactions generating strand breaks, mainly involving reactive radical intermediates, and the direct photochemical process leading to UV-photoproducts. Thus, localized multi-photon excitation with a wavelength longer than 1 μm allows for the selective production of DNA strand breaks at submicrometer spatial resolution in the absence of photosensitizers.

INTRODUCTION

Techniques to induce local DNA damage in the nuclei of living cells have been pivotal to the elucidation of DNA repair mechanisms, principally those responding to UV-mediated lesions. Discrete sites of damage were generated either via focusing of UV lasers (1,2) or by globally irradiating cell monolayers through polycarbonate filters with pores of defined size as a shadow mask (3). These studies allowed for the spatiotemporal analysis of the nucleotide excision repair (NER) pathway (4). In order to exploit these techniques also for the study of DNA double strand break (DSB) repair that is mainly mediated by homologous recombination (HR) and non-homologous end joining (NHEJ), two variants were introduced: the first relies on the expression of an exogenous UV-damage endonuclease that introduces single strand breaks at the sites of UV lesions (5). The second, more widespread procedure consists in preincubating the cells with sensitizers like the thymidine analog bromodeoxyuridine (BrdU) and/or the DNA intercalating drug Hoechst (6–9). Drawbacks of these methods are the necessity to create endonuclease-expressing cell lines and the unwanted side effects of the sensitizers (10). Furthermore, the specificity of these techniques has been questioned by reports showing that in the presence of sensitizers, also cyclobutane-pyrimidine dimers (CPDs) are formed in addition to the desired DSBs (11).

Recently, irradiation with pulsed femtosecond lasers in the near infrared has emerged as a powerful technique to generate DNA damage at high spatial resolution (12). The main advantages consist in the 3D confinement of the lesions and the reduced phototoxicity. Several studies on the dynamics of DNA repair proteins in living cells have employed Ti : sapphire femtosecond lasers emitting around 800 nm. First reported as being an efficient inducer of CPDs, multiphoton absorption at this wavelength has meanwhile been shown to generate a broad spectrum of lesions including 6-4 photoproducts (6-4 PPs) and DSBs (11,13). The lack of specificity poses a strong limitation to this method as a tool to study individual DNA repair pathways in living cells.

Prompted by a recent report showing that a wavelength shift of 18 nm in the UV range of the spectrum (from 312 to 330 nm) drastically influenced the nature of the UV-photoproducts generated by linear absorption (14) we asked whether the outcome of multiphoton excitation in the near infrared could also be influenced by modifying the excitation wavelength. To our knowledge, no data are available so far on DNA photodamage by infrared irradiation beyond 800 nm. Taking advantage of the ultrabroadband tunability of our femtosecond laser source (15) we have therefore compared DNA damage induction at two wavelengths in the near infrared, namely 775 and 1050 nm. A quantitative analysis of the power dependence of different types of DNA lesions allowed us to identify conditions that specifically favor DSBs with respect to UV photoproducts. With the increasing commercial availability of tunable femtosecond lasers this method can be easily employed in non-specialized laboratories as a tool to selectively induce

*To whom correspondence should be addressed. Tel: +49 7531 884054; Fax: +49 7531 4005; Email: elisa.may@uni-konstanz.de

DSBs in the absence of sensitizers and at high spatial resolution.

MATERIALS AND METHODS

Cell culture procedures

HeLa 229 cells were grown in Dulbecco's modified Eagle's Medium (Invitrogen) supplemented with 10% fetal calf serum (FCS), and 100 U/ml penicillin–streptomycin. For microscopy experiments cells were seeded in grid-500 dishes (Ibidi) to allow for easy identification of irradiated cells. For XRCC1–GFP expression, Hela cells were transfected with Effectene (Qiagen) according to the manufacturer's instructions.

Antibodies and immunocytochemistry

Cells were fixed immediately after laser irradiation in PBS containing 4% paraformaldehyde for 15 min. For the detection of UV-photoproducts (this term indicates CPDs and 6-4 PPs), cells were extensively washed in PBS containing 0.1 % Tween 20 (PBS/Tween) followed by DNA denaturation in a 0.07 M NaOH solution in PBS for 8 min. After several washing steps in PBS/Tween, cells were incubated in 20% FCS in PBS for 30 min. Antibody incubations occurred overnight at 4°C. The α-6–4 PP antibody (MBL) was diluted 1 : 3000, the α-CPD antibody (MBL) was diluted 1 : 1000 in PBS containing 5% FCS. Alexa Fluor 568-conjugated goat α-mouse immunoglobulins (Molecular Probes) were used as secondary antibody. DNA was counterstained with Hoechst 33342 (200 ng/μl). For the detection of H2AX phosphorylation, cells were treated after fixation for 10 min with PBS containing 50 mM NH_4Cl, washed in PBS and permeabilized with 0.2% Triton-X-100 in PBS for 5 min. After incubation in a 1% solution of bovine serum albumin (BSA) in PBS, mouse α-γH2AX antibody (Upstate) was applied at a dilution of 1 : 500 in PBS containing 10% normal goat-serum (Sigma Aldrich).

Detection of reactive oxygen species

Cells were washed twice with PBS prewarmed at 37°C followed by incubation in PBS containing 10 μM 5,6-Chloromethyl-2′,7′-dichlorodihydrofluorescein-diacetate (CM-H_2DCFDA) (Molecular Probes) for 40 min on the microscope stage heated to 37°C. After two washing steps with prewarmed PBS, cells were irradiated, leading to reactive oxygen species (ROS) formation and oxidation of CM-H_2DCFDA to its fluorescent form 5,6-Chloromethyl-2′,7′-dichlorofluorescein (5,6-CM-2′,7′-DCF) (16). For quenching experiments, N-acetyl-cysteine (Sigma-Aldrich) was added at 4 mM concentration. Imaging of ROS-specific signals occurred as described below.

DNA damaging and imaging setup

Our setup consists of a Pascal 5 laser scanning microscope from Carl Zeiss and a widely tunable femtosecond Er : fiber system (15). The pulse repetition rate is 107 MHz. In order to further increase the average output power in the wavelength regime beyond 1000 nm, an Yb : fiber amplifier stage was added. This combination provides a train of pulses with a duration of 77 fs at a wavelength of 1050 nm. In addition, the laser provides 230 fs pulses at 775 nm via frequency doubling of an Er : fiber amplifier. This wavelength serves to establish comparison to previous work carried out with Ti : sapphire lasers. All pulse durations given were determined in the focal plane of the microscope. They were measured by interferometric autocorrelation using a home-built device (15). Similar autocorrelators for pulse diagnostics in the focal plane of microscope systems are commercially available. The objective lens used for the induction of DNA damage as well as for the subsequent imaging is a 40× oil immersion lens with a numerical aperture of 1.3 (EC-Plan-Neo-Fluar, Carl Zeiss). At a wavelength of 775 nm, the full widths at half maximum (FWHM) of the point spread function (PSF) for two-photon excitation of subresolution-size fluorescent beads (PS-Speck, 175 nm, Molecular Probes, Invitrogen) were $d = 270$ nm in lateral and $a = 590$ nm in axial direction. For 1050 nm we found a lateral width of $d = 377$ nm and an axial extension of $a = 1.4$ μm.

The average power after transmission through the microscope was measured with a calibrated large-area photodiode (S130 A, Thorlabs). To avoid errors due to internal reflections, immersion oil was applied between the objective lens and the large-area photodiode. This method was double checked by employing a double transmission technique. To this end a mirror was placed in the focal plane to retroreflect the beam. Before the microscope a beam splitter was inserted to quantify the reflected irradiation with a thermal power meter. Both measurements yielded identical transmission values. Artifacts due to nonlinear absorption were avoided by working well beyond the focal plane. The following equation was used to calculate the peak irradiance: $I_{peak} = P_{av}/(f_{rep} \times \tau \times \pi \times r^2)$. f_{rep} is the pulse repetition rate of our system, τ the pulse duration (FWHM of the intensity) and r is the radius of the irradiated spot, determined by the two-photon nonlinear characterization as $r = \sqrt{2} \times d/2$.

For excitation at 775 nm we reached a peak irradiance of 312 GW/cm^2 in the focal plane. The maximum intensity at a wavelength of 1050 nm amounts to 1200 GW/cm^2. The pixel dwell time was set to 44.2 ms and two crossed lines were irradiated in each experiment. Each line was 10 μm in length, corresponding to 76 pixels. The cross is a clearly distinguishable pattern that does not exist in untreated cells. It is therefore preferred to spot-like patterns. The dimension of the exposed volume was 38 fl, as estimated from the line length (10 μm) and the axial extension of the PSF determined above. We note that this value refers to a two-photon absorption process. The actual DNA damage requires higher-order nonlinear interactions. Therefore it is confined to an even smaller volume.

XRCC1–GFP accumulation at the site of damage and 5,6-CM-2′,7′-DCF generation were detected using the 488 nm line of the CW Ar-ion laser provided with the LSM 5 Pascal. An initial control image was taken

immediately before damage induction. A second image was taken 64 s after irradiation. This frame was subsequently employed for signal quantification. Minimum laser power was employed to avoid acquisition bleaching. Immunofluorescence signals were visualized with a Zeiss Axiovert 200 M microscope using epi-illumination with proper excitation and emission filters and keeping identical microscope and camera settings between experiments.

Image analysis

Quantification of fluorescence images was performed with ImageJ (http://rsb.info.nih.gov/ij). For evaluation of XRCC1–GFP accumulation (Figure 3), the average fluorescence intensity was analyzed in the area of accumulation. To account for varying expression levels a neighboring area of identical size was taken as reference.

For quantification of immunocytochemistry experiments, the average intensity was measured in a region of interest encompassing the damage-specific signal and in a reference area within the same cell. In the latter experiments, XRCC1–GFP signals served as positive controls to identify the damaged region in cells with weak or no staining.

RESULTS

Experimental setup

We extended a confocal microscopy setup consisting of a femtosecond Er : fiber laser coupled to a Carl Zeiss LSM 5 Pascal laser scanning microscope (15) by adding a Yb : fiber amplifier (Figure 1). This device delivers output spectra centered at 1050 nm with a bandwidth of up to 50 nm (FWHM). After pulse compression we achieve a pulse duration of 77 fs. The system is used to irradiate nuclei of live HeLa cells at 775 and 1050 nm. Details about the imaging parameters are given in 'Materials and Methods' section.

Recruitment of XRCC1 after femtosecond laser irradiation at 775 and 1050 nm

To achieve a quantitative comparison of the effects caused by the two excitation wavelengths we first sought to identify irradiation conditions that trigger a similar level of response of the DNA repair machinery. As an indicator we choose the DNA repair factor XRCC1, which is sensitive to a broad spectrum of lesions, mostly substrates of the base-excision repair (BER) pathway (17,18).

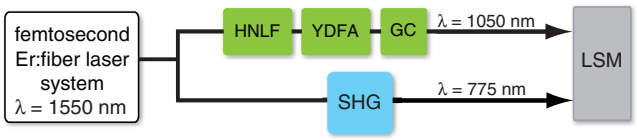

Figure 1. Schematic of the setup used for DNA microdamage, consisting of a femtosecond Er:fiber laser system, a periodically poled lithium niobate crystal for second harmonic generation (SHG), a highly nonlinear germanosilicate fiber (HNLF) for generation of a tailored supercontinuum and a Yb:fiber amplifier (YDFA) with subsequent grating compressor (GC). The microscope is a laser scanning confocal LSM 5 Pascal from Carl Zeiss.

More recently, it was also shown that XRCC1 is involved in NER (19). We monitored the accumulation of an XRCC1–GFP fusion at the site of femtosecond laser exposure in nuclei of HeLa cells using different peak irradiance values at 775 and 1050 nm. XRCC1–GFP readily aggregates at damaged sites in live HeLa cells at both wavelengths. The spot of accumulation is restricted to the focal region as expected for a nonlinear absorption process (Figure 2).

Signal quantification revealed that ~3 times higher peak powers are necessary at 1050 nm to achieve recruitment levels comparable to 775 nm. This finding may be explained by the higher number of photons involved in each elementary absorption event that is required at 1050 nm owing to the lower quantum energy. The damage yield as a function of irradiation intensity and wavelength is shown in Figure 3. We find different initial slopes of the power dependence of 4.9 ± 2.1 for excitation at 775 nm and of 8.3 ± 4.0 at 1050 nm, respectively. This result directly supports our interpretation of a higher-order nonlinear absorption process for the case of longwave excitation.

Interestingly, we observed the onset of some saturation behavior for peak intensities above 300 GW/cm^2 at 775 nm and 900 GW/cm^2 at 1050 nm. In this regime, a threshold for maximum accumulation of XRCC1 became apparent, suggesting a comparably high density of DNA lesions at the two wavelengths. We therefore choose these conditions for the following experiments aimed at the characterization and quantitative comparison of the different types of underlying DNA damage.

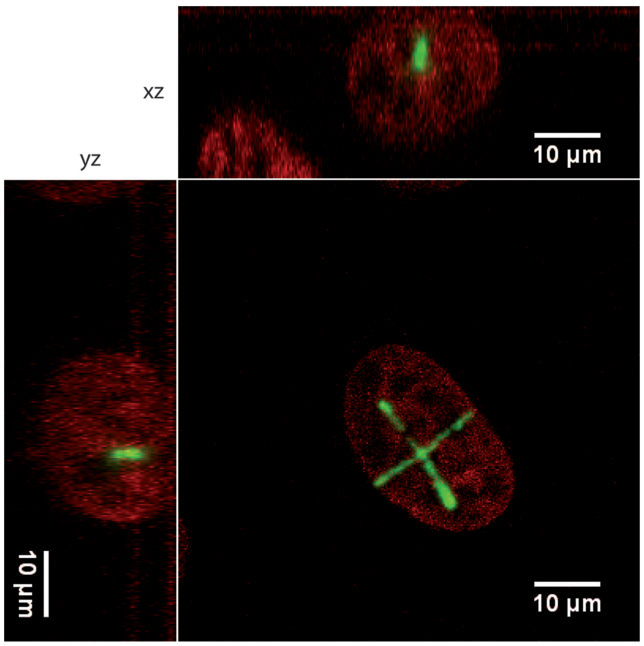

Figure 2. XRCC1–GFP accumulates at irradiated sites in HeLa cell nuclei. HeLa cells expressing an XRCC1–GFP fusion were irradiated with the Er/Yb : fiber laser tuned to 1050 nm along two intersecting lines. The cells were fixed within 1 min after irradiation and imaged subsequently by confocal microscopy. The orthogonal projections highlight the spatial confinement of the XRCC1–GFP signal. Green: XRCC1–GFP. Red: Hoechst 33342.

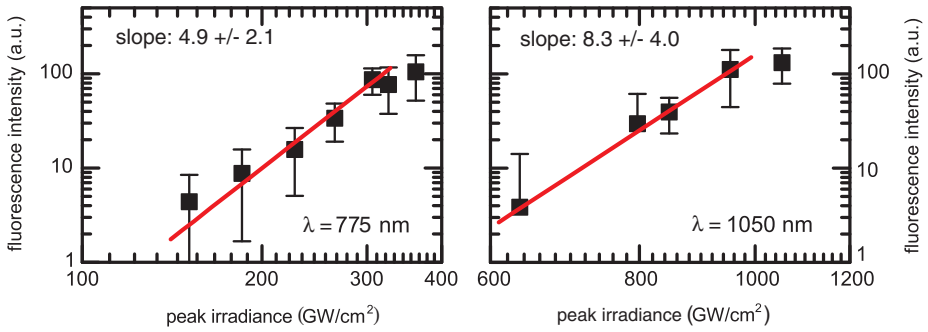

Figure 3. Dependence of XRCC1 accumulation at 775 and 1050 nm from irradiance. Quantitative analysis of images of XRCC1–GFP expressing HeLa cells exposed to femtosecond pulses at 775 and 1050 nm as shown in Figure 2. Images were taken 64 s after irradiation at different peak irradiance values. The results are plotted on a double logarithmic scale. A linear function was fitted and the resulting slopes are 4.9 ± 2.1 at 775 nm and 8.3 ± 4.0 at 1050 nm. For each data point the accumulation of at least 10 cells was averaged. Error bars show standard deviation.

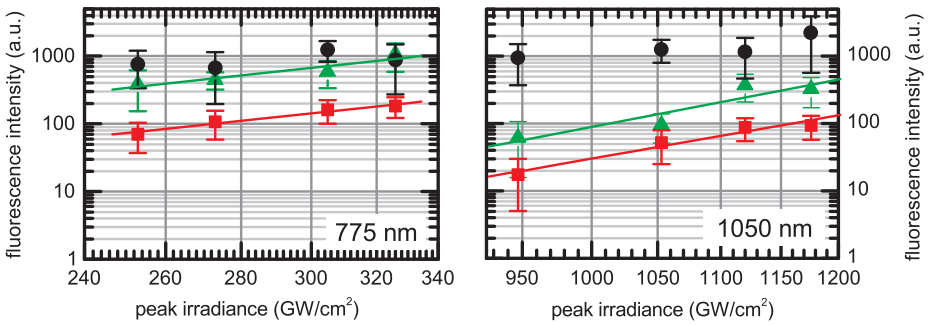

Figure 4. Dependence of signals specific for γH2AX (black circles), CPDs (green triangles) and 6-4 PPs (red squares) on the peak irradiance. Note that both axes are plotted on a logarithmic scale. Error bars show the standard deviation. Each data point represents the average value from at least eight cells. The slopes for a linear fit are 3.7 ± 0.9 (CPDs) and 3.8 ± 0.5 (6-4 PPs) at 775 nm, and 8.9 ± 2.6 (CPDs) and 8.1 ± 1.2 (6-4 PPs) at 1050 nm.

Differential dependence of UV photoproducts and DSBs on irradiance at 775 and 1050 nm

Next, we investigated the power dependence of three types of lesions, namely DSBs, CPDs and 6-4 PPs. Phosphorylation of histone H2AX was taken as an established indicator for DSBs, while UV photoproducts were detected directly via specific antibodies. After excitation with the femtosecond laser at the irradiance values determined above, DNA damage was detected by immunocytochemistry and the corresponding signals were quantified.

Comparison of the power dependence of the signals reflecting the different DNA lesions revealed that the level of H2AX phosphorylation is similar and saturated, not varying significantly at both wavelengths. In contrast, a marked difference is observed in the case of UV photoproducts which decrease significantly at 1050 nm. Thus, the ratio between DNA strand breaks and UV photoproducts is nearly one order of magnitude larger at 1050 nm as compared to 775 nm at the lowest irradiation power. In addition, the power-dependent increase of photoproduct induction is more pronounced at 1050 nm than at 775 nm (Figure 4). As a result, a regime around 950 GW/cm^2 is identified for excitation at 1050 nm that allows for highly selective generation of DSBs. Direct visualization of the immunocytochemical labeling of HeLa cells irradiated either at 775 nm (253 GW/cm^2) or at 1050 nm (947 GW/cm^2) independently confirms this conclusion: at the shorter wavelength, signals specific for γH2AX, CPDs and 6-4 PPs are readily observable, while at 1050 nm the photoproduct-specific signals fall below the detection limit (Figure 5).

ROS contribute to the generation of DSBs by femtosecond laser irradiation

ROS are an accepted source of multiple DNA alterations including DSBs in cells treated with various genotoxins or subjected to radiative exposure (X-rays, UV) (20–23). On the other hand, femtosecond laser irradiation was reported to produce ROS in live cells (24).

In order to explore the role of ROS in our system, we monitored their production using the fluorescent indicator CM-H_2DCFDA. Excitation both at 775 nm (326 GW/cm^2) and 1050 nm (800 GW/cm^2) leads to a fluorescent signal localized along the laser path. This signal was effectively quenched in presence of the scavenger *N*-acetylcysteine (NAC) (Figure 6A).

To answer the question as to whether ROS production correlates with the induction of DSBs we choose irradiation conditions at 775 and 1050 nm that would induce different amounts of ROS and measured the respective levels of γH2AX-specific signal produced under the same conditions. Signal quantification shows a highly significant correlation between the level of ROS and that of γH2AX, strongly indicating that oxygen radicals

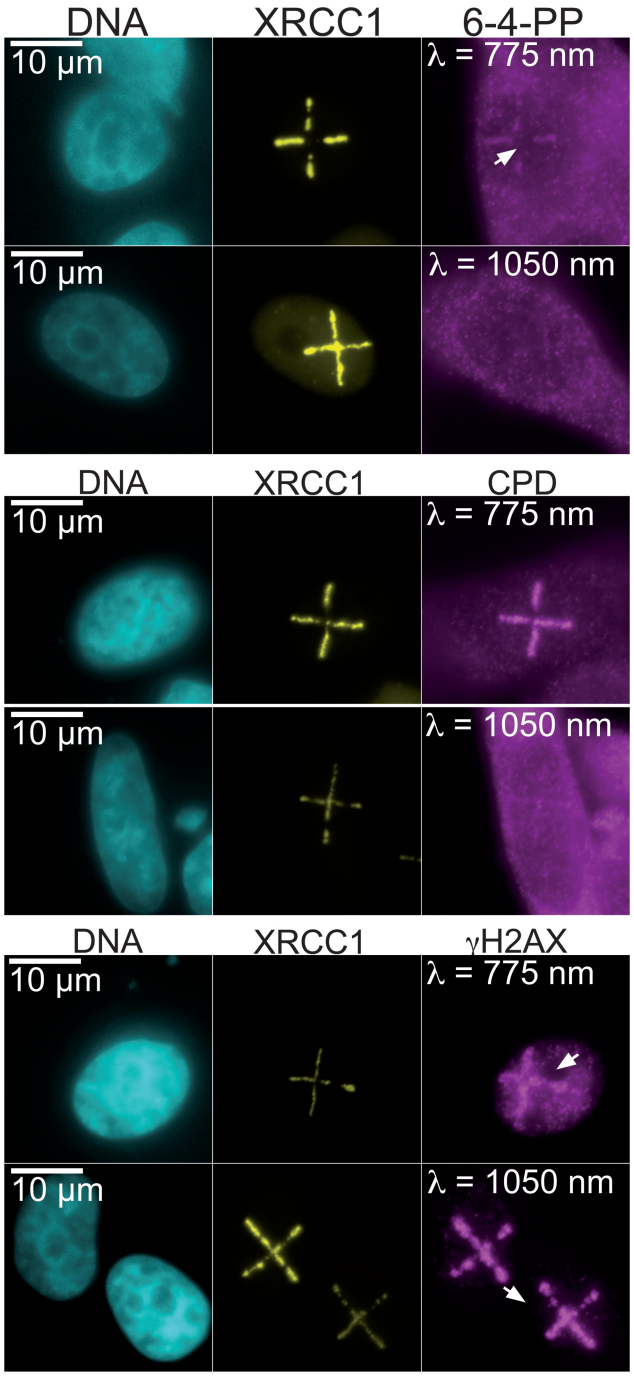

Figure 5. Femtosecond laser pulses at 1050 nm selectively induce DSBs in HeLa cell nuclei. Immunocytochemical analysis of HeLa cells expressing XRCC1–GFP. Cells were irradiated at 775 nm (253 GW/cm^2) or 1050 nm (947 GW/cm^2), fixed and labeled with antibodies specific for γH2AX, CPDs and 6-4 PPs. The XRCC1–GFP signal served as a positive control and allowed to identify the irradiated region.

contribute to the formation of DSBs in our experimental system (Figure 6B).

DISCUSSION

Purpose of this study was to determine which types of lesions are induced when cellular DNA is irradiated *in situ* with infrared femtosecond laser pulses and whether the result may be influenced by the excitation wavelength. In a recent investigation, Dinant *et al.* (11), have compared pulsed 800 nm with focused UV-C (266 nm) and with 405 nm irradiation, the latter combined with Hoechst 33342 sensitization. At 266 nm they can identify conditions that selectively generate UV-photoproducts but no DSBs, as judged by the exclusive recruitment of NER repair factors to the site of damage. The other two regimes were shown to produce a broad variety of DNA lesions as well as aberrant reactions, leading the authors to conclude that 'the selective induction of DNA strand breaks cannot be achieved with currently existing laser-assisted damaging methods'. Similar results were reported recently by Kong and coworkers (13). However, the potential of wavelengths beyond 800 nm has not been explored so far. Here, we have employed our broadly tunable Er/Yb:fiber laser to quantitatively compare the effects of femtosecond laser pulses at 775 and 1050 nm. Our data show that increasing the wavelength beyond the maximum of three-photon absorption for DNA (~3 times $\lambda_{max,\,linear}$ 260 nm) strongly decreases the efficiency of UV photoproduct formation. Under the same conditions, DNA strand breaks are still produced at high levels. The net result is an increase in the yield of DNA strand breaks by more than one order of magnitude when the irradiation power is chosen appropriately. The optimum selectivity is achieved at a peak intensity of 950 GW/cm^2 for an excitation wavelength of 1050 nm. We show a representative image of a damaged nucleus, displaying a bright γH2AX-specific signal and no detectable UV-photoproducts in Figure 5.

The different behavior of the two investigated wavelengths with respect to their ability to damage DNA may be interpreted in terms of the distinct mechanisms involved. CPDs and 6-4 PP are products of a chemical reaction induced by direct multiphoton excitation of DNA that has its maximum of linear absorption in the UV-C range at around 260 nm (corresponding to a photon energy of 4 eV). Therefore, the same transition requires three photons at 775 nm (photon energy of 1.6 eV) and four photons at 1050 nm (corresponding to 1.18 eV per quantum of light). As a result, high photon fluxes above 1050 GW/cm^2 are needed at the longer wavelength in order to produce a significant amount of UV photoproducts. In addition, due to the fourth power dependence of the reaction, the efficiency of multiphoton absorption decreases more rapidly at 1050 nm than at 775 nm (compare the graphs in Figure 4).

In strong contrast to UV-photoproducts, DSBs are formed after pulsed infrared irradiation via indirect mechanisms involving ionic and radical intermediates. Femtosecond laser excitation of biomaterials was shown to generate free electrons by low-density plasma formation over a broad range of conditions (25). The chemical processes triggered by free electrons are discussed as one major source of DSBs in the spatially extremely confined irradiation region (13). In the presence of water, this involves the production of solvated electrons (26) and multiple reactive intermediates such as superoxide,

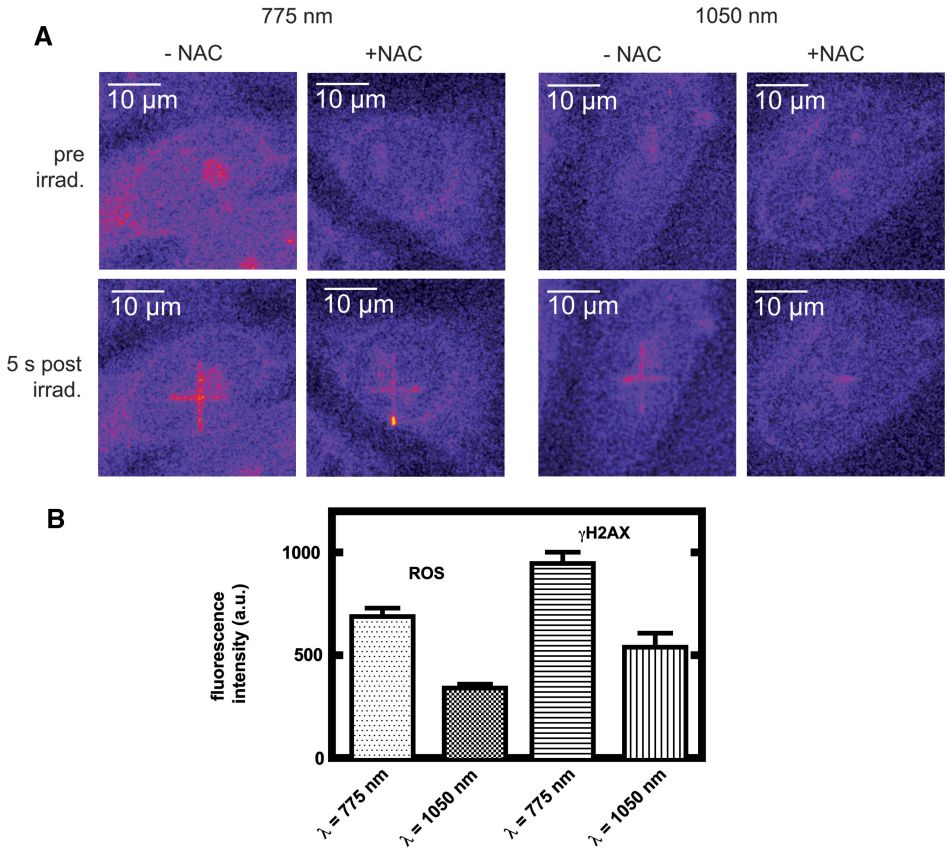

Figure 6. ROS contribute to DNA strand breaks induced by femtosecond irradiation. (**A**) HeLa cells were incubated with CM-H_2DCFDA before excitation at 775 nm (326 GW/cm^2) and 1050 nm (800 GW/cm^2). Images taken prior to and immediately after exposure are shown. As a control, cells were pre-treated with 4 mM NAC. NAC effectively quenches the ROS-specific signal. (**B**) Irradiation conditions were chosen such as to generate ~50% less ROS at 1050 nm as compared to 775 nm. Cells were irradiated in parallel experiments, monitored for the production of ROS and labeled with a γH2AX-specific antibody. The effect on the γH2AX-specific signal correlates quantitatively with the decrease in ROS. Data points are an average of at least 34 cells. Error bars show standard error of the mean.

hydroxyl and peroxyl radicals (27,28). Solvated electrons *per se* were shown to attack DNA in aqueous buffered solution (29). The production of ROS in live cells by 800 nm femtosecond pulses has also been demonstrated (24). In the present study, we show a quantitative correlation between ROS levels and H2AX phosphorylation. These reactions exhibit high cross-sections because of the high concentration of water and polar species (nucleotides, proteins, salts) in the nuclear environment. In addition, laser-driven plasma generation and multiphoton photodissociation are processes beyond the regime of perturbative nonlinear optics where the efficiency depends less on photon energy but on the peak electric field of the optical wave (25). On the other hand, the finite time it takes reactive species to diffuse toward the DNA in combination with the onset of bimolecular recombination limits the increase of damage with irradiation intensity at some point. In our experiments we observed saturating levels of the DSB indicator at both excitation wavelengths applied. Exploiting the increasing power dependence of UV photoproducts at longer wavelengths, we were able to identify conditions that allow for the selective production of DSBs at 1050 nm.

Oxidized bases, such as 8-oxoguanine, were not observed in our experiment (data not shown). This result is in agreement with data recently published by Kong *et al.* (13). These authors detected oxidative base damage after UV-A microirradiation but not with femtosecond pulses at a wavelength of 800 nm. In addition, a fluorescently tagged fusion of 8-oxoguanine-glycosylase (OGG1), the repair enzyme responsible for excision of 8-oxo-G, failed to accumulate at irradiated sites (data not shown). We conclude that under our experimental conditions, the generation of oxidative base damage is negligible as compared to DSB induction.

Different to the findings by Tirlapur *et al.* (24), we do not observe nuclear fragmentation and cell death under our irradiation conditions (data not shown). Still, we found ROS production both at 775 and 1050 nm. A discrepancy with the results of Hockberger *et al.* (30), who did not detect ROS at 1047 nm may be explained by the lower peak irradiance (estimated to be about 3 times lower, i.e. <350 GW/cm^2) and the shorter pixel dwell times employed in their study. On the other hand, our parameters settle well below those used for intracellular dissection and cell transfection (25), both methods that introduce cell injury.

In sum, we propose a method for localized femtosecond irradiation of live cell nuclei that introduces DSBs with high selectivity and minimum phototoxicity. The ability to induce selective damage with sub-micrometer spatial resolution in three dimensions represents a significant advantage over more conventional methods such as treatment with X-rays or α-particles. We expect that further optimization of the parameters excitation wavelength, pulse duration and peak intensity will improve the discriminatory potential of this method for various types of damage.

SUPPLEMENTARY DATA

Supplementary Data are available at NAR Online.

ACKNOWLEDGEMENTS

The authors thank Daniela Hermann for expert technical assistance, Sebastian Seibel for ROS staining and Claudia Lukas for XRCC1–GFP expressing plasmid.

FUNDING

Center for Applied Photonics at University of Konstanz; The Ministry of Science, Research and the Arts of Baden-Württemberg. Funding for open access charge: Center for Applied Photonics, University of Konstanz, Germany.

Conflict of interest statement. None declared.

REFERENCES

1. Cremer,C., Cremer,T., Fukuda,M. and Nakanishi,K. (1980) Detection of laser–UV microirradiation-induced DNA photolesions by immunofluorescent staining. *Hum. Genet*., **54**, 107–110.
2. Cremer,C., Cremer,T. and Jabbur,G. (1981) Laser–UV-microirradiation of Chinese hamster cells: the influence of the distribution of photolesions on unscheduled DNA synthesis. *Photochem. Photobiol*., **33**, 925–928.
3. Mone,M.J., Volker,M., Nikaido,O., Mullenders,L.H., van Zeeland,A.A., Verschure,P.J., Manders,E.M. and van Driel,R. (2001) Local UV-induced DNA damage in cell nuclei results in local transcription inhibition. *EMBO Rep*., **2**, 1013–1017.
4. Volker,M., Mone,M.J., Karmakar,P., van Hoffen,A., Schul,W., Vermeulen,W., Hoeijmakers,J.H.J., van Driel,R., van Zeeland,A.A. and Mullenders,L.H.F. (2001) Sequential assembly of the nucleotide excision repair factors in vivo. *Mol. Cell*, **8**, 213–224.
5. Okano,S., Lan,L., Caldecott,K.W., Mori,T. and Yasui,A. (2003) Spatial and temporal cellular responses to single-strand breaks in human cells. *Mol. Cell Biol*., **23**, 3974–3981.
6. Limoli,C.L. and Ward,J.F. (1993) A new method for introducing double-strand breaks into cellular DNA. *Radiat. Res*., **134**, 160–169.
7. Walter,J., Cremer,T., Miyagawa,K. and Tashiro,S. (2003) A new system for laser–UVA-microirradiation of living cells. *J. Micro. Oxford*, **209**, 71–75.
8. Lukas,C., Falck,J., Bartkova,J., Bartek,J. and Lukas,J. (2003) Distinct spatiotemporal dynamics of mammalian checkpoint regulators induced by DNA damage. *Nat. Cell Biol*., **5**, 255–260.
9. Harper,J.V., Reynolds,P., Leatherbarrow,E.L., Botchway,S.W., Parker,A.W. and O'Neill,P. (2008) Induction of persistent double strand breaks following multiphoton irradiation of cycling and G1-arrested mammalian cells-replication-induced double strand breaks. *Photochem. Photobiol*., **84**, 1506–1514.
10. Lukas,C., Bartek,J. and Lukas,J. (2005) Imaging of protein movement induced by chromosomal breakage: tiny 'local' lesions pose great 'global' challenges. *Chromosoma*, **114**, 146–154.
11. Dinant,C., de Jager,M., Essers,J., van Cappellen,W.A., Kanaar,R., Houtsmuller,A.B. and Vermeulen,W. (2007) Activation of multiple DNA repair pathways by subnuclear damage induction methods. *J. Cell Sci*., **120**, 2731–2740.
12. Meldrum,R.A., Botchway,S.W., Wharton,C.W. and Hirst,G.J. (2003) Nanoscale spatial induction of ultraviolet photoproducts in cellular DNA by three-photon near-infrared absorption. *EMBO Rep*., **4**, 1144–1149.
13. Kong,X., Mohanty,S., Stephens,J., Heale,J., Gomez-Godinez,V., Shi,L., Kim,J., Yokomori,K. and Berns,M. (2009) Comparative analysis of different laser systems to study cellular responses to DNA damage in mammalian cells. *Nucleic Acids Res*., **37**, e68.
14. Mouret,S., Baudouin,C., Charveron,M., Favier,A., Cadet,J. and Douki,T. (2006) Cyclobutane pyrimidine dimers are predominant DNA lesions in whole human skin exposed to UVA radiation. *Proc. Natl Acad. Sci. USA*, **103**, 13765–13770.
15. Träutlein,D., Adler,F., Moutzouris,K., Jeromin,A., Leitenstorfer,A. and Ferrando-May,E. (2008) Highly versatile confocal microscopy system based on a tunable femtosecond Er:fiber source. *J. Biophotonics*, **1**, 53–61.
16. Hempel,S.L., Buettner,G.R., O'Malley,Y.Q., Wessels,D.A. and Flaherty,D.M. (1999) Dihydrofluorescein diacetate is superior for detecting intracellular oxidants: Comparison with 2′,7′-dichlorodihydrofluorescein diacetate, 5(and 6)-carboxy-2′, 7′-dichlorodihydrofluorescein diacetate, and dihydrorhodamine 123. *Free Rad. Biol. Med*., **27**, 146–159.
17. Mortusewicz,O. and Leonhardt,H. (2007) XRCC1 and PCNA are loading platforms with distinct kinetic properties and different capacities to respond to multiple DNA lesions. *BMC Mol. Biol*., **8**, 81.
18. Campalans,A., Marsin,S., Nakabeppu,Y., O'Connor,T.R., Boiteux,S. and Radicella,J.P. (2005) XRCC1 interactions with multiple DNA glycosylases: A model for its recruitment to base excision repair. *DNA Repair*, **4**, 826–835.
19. Moser,J., Kool,H., Giakzidis,I., Caldecott,K., Mullenders,L.H. and Fousteri,M.I. (2007) Sealing of chromosomal DNA nicks during nucleotide excision repair requires XRCC1 and DNA ligase III alpha in a cell-cycle-specific manner. *Mol. Cell*., **27**, 311–323.
20. Von Sonntag,C. (2006) *Free Radical Induced DNA Damage and Its Repair*. Springer, Berlin Heidelberg.
21. Tominaga,H., Kodama,S., Matsuda,N., Suzuki,K. and Watanabe,M. (2004) Involvement of reactive oxygen species (ROS) in the induction of genetic instability by radiation. *J. Rad. Res*., **45**, 181–188.
22. Bjelland,S. and Seeberg,E. (2003) Mutagenicity, toxicity and repair of DNA base damage induced by oxidation. *Mutat. Res*., **531**, 37–80.
23. Friedberg,E.C., Walker,G.C., Siede,W., Wood,R.D., Schultz,R.A. and Ellenberger,T. (2006) *DNA Repair and Mutagenesis*, 2nd edn. ASM Press, Washington D.C.
24. Tirlapur,U.K. (2001) Femtosecond near-infrared laser pulses elicit generation of reactive oxygen species in mammalian cells leading to apoptosis-like death. *Exp. Cell Res*., **263**, 88–97.
25. Vogel,A., Noack,J., Huttman,G. and Paltauf,G. (2005) Mechanisms of femtosecond laser nanosurgery of cells and tissues. *App. Phys. B-Las. Optics*, **81**, 1015–1047.
26. Assel,M., Laenen,R. and Laubereau,A. (2000) Femtosecond solvation dynamics of solvated electrons in neat water. *Chem. Phys. Lett*., **317**, 13–22.
27. Nikogosyan,D.N., Oraevsky,A.A. and Rupasov,V.I. (1983) 2-Photon ionization and dissociation of liquid water by powerful laser UV-radiation. *Chem. Phys*., **77**, 131–143.
28. Bisby,R.H., Crisostomo,A.G., Botchway,S.W. and Parker,A.W. (2009) Nanoscale hydroxyl radical generation from multiphoton ionization of tryptophan. *Photochem. Photobiol*., **85**, 353–357.
29. Schussler,H., Navaratnam,S. and Distel,L. (2005) Rate constants for the reactions of DNA with hydrated electrons and with OH-radicals. *Radiat. Phys. Chem*., **73**, 163–168.
30. Hockberger,P.E., Skimina,T.A., Centonze,V.E., Lavin,C., Chu,S., Dadras,S., Reddy,J.K. and White,J.G. (1999) Activation of flavin-containing oxidases underlies light-induced production of H2O2 in mammalian cells. *Proc. Natl Acad. Sci. USA*, **96**, 6255–6260.